Composition Dependence of the Crystallization Behavior and Morphology of the Poly(ethylene oxide)-poly(ϵ-caprolactone) Diblock Copolymer

Chaoliang He,[†,‡] Jingru Sun,[†] Jia Ma,[†] Xuesi Chen,*[,†,‡] and Xiabin Jing[†,‡]

State Key Laboratory of Polymer Physics and Chemistry, Changchun Institute of Applied Chemistry, Chinese Academy of Sciences, Changchun 130022, P. R. China and Graduate School of Chinese Academy of Sciences, Beijing 100039, P. R. China

Received June 16, 2006; Revised Manuscript Received September 18, 2006

The crystallization behavior and morphology of the crystalline−crystalline poly(ethylene oxide)-poly(ϵ-caprolactone) diblock copolymer (PEO-b-PCL) was studied by differential scanning calorimetry (DSC), wide-angle X-ray diffraction (WAXD), Fourier transform infrared spectroscopy (FTIR), small-angle X-ray scattering (SAXS), and hot-stage polarized optical microscope (POM). The mutual effects between the PEO and PCL blocks were significant, leading to the obvious composition dependence of the crystallization behavior and morphology of PEO-b-PCL. In this study, the PEO block length was fixed (M_n = 5000) and the weight ratio of PCL/PEO was tailored by changing the PCL block length. Both blocks could crystallize in PEO-b-PCL with the PCL weight fraction (WF_{PCL}) of 0.23−0.87. For the sample with the WF_{PCL} of 0.36 or less, the PEO block crystallized first, resulting in the obvious confinement of the PCL block and vice versa for the sample with WF_{PCL} of 0.43 or more. With increasing WF_{PCL}, the crystallinity of PEO reduced continuously while the variation of the PCL crystallinity exhibited a maximum. The long period of PEO-b-PCL increased with increasing WF_{PCL} from 0.16 to 0.50 but then decreased with the further increase of WF_{PCL} due to the interaction of the respective variation of the thicknesses of the PEO and PCL crystalline lamellae. Only the PEO spherulites were observed in samples with WF_{PCL} of 0.16−0.36 by POM, in contrast to only the PCL spherulites in samples with WF_{PCL} of 0.56−0.87. For samples with WF_{PCL} of 0.43 and 0.50, a unique concentric spherulite was observed. The morphology of the inner and outer portions of the concentric spherulites was determined by the PCL and PEO spherulites, respectively. The growth rate of the PEO spherulites reduced rapidly with increasing WF_{PCL} from 0 to 0.50. However, when increasing WF_{PCL} from 0.43 to 0.87, the variation of the growth rate of the PCL spherulites exhibited a maximum rather than a monotonic change.

1. Introduction

The biodegradable and biocompatible aliphatic polyesters, such as poly(ϵ-caprolactone) (PCL), poly(lactic acid), poly(glycolic acid), and their copolymers and blends have received worldwide attention for their potential applications in the biomedical materials and as environmentally friendly materials.[1,2] The synthesis of the biodegradable polyesters has been extensively developed.[3,4] At the same time, more and more attention has focused on their physical properties, especially the mechanical properties, crystallization behavior, and morphology, which were directly related to their industrial applications and degradation behaviors.[5−14] Recently, poly(ethylene oxide)-poly(ϵ-caprolactone) (PEO-PCL) block copolymers were developed for their unique properties, such as biocompatibility, amphiphilicity, self-assembly, permeability, and controllable biodegradability.[15] It was established that the crystallinity had a significant effect on both drug permeability and biodegradation behavior.[16] However, the crystallization behavior of the block copolymer containing two crystallizable blocks[17−32] may be more complicated than that of the crystalline−amorphous block copolymer.[33−37] Nojima et al.[21] studied the morphology of the PCL-PEO-PCL triblock copolymers. It was concluded that the PEO and PCL crystals existed independently and there was no eutectic crystal of two components. Gan et al.[22,23] studied the isothermal crystallization and melting behavior of the PEO-PCL diblock copolymer with the PEO weight fraction of 0.20. It was found that PEO could hardly crystallize within the diblock copolymer. Floudas et al.[24] studied the crystallization behaviors of poly(styrene)-PEO-PCL (PS-PEO-PCL) triarm star block copolymers. It was suggested that the microphase segregation was driven by the crystallization driving force of one or both crystalline blocks. Bogdanov et al.[25,26] characterized the thermal properties of three types of PEO-PCL block copolymers with WF_{PCL} of 0.68−0.81. It was established that the PCL block crystallized first and fixed the total structure of the spherulites, leading to significant imperfect crystallization of the PEO block. Shiomi et al.[27] observed a unique double concentric spherulite such as concentric circles for the PCL-PEO-PCL triblock copolymers with WF_{PCL} of 0.60 and 0.66. Muller et al.[28] studied the crystallization behavior of PS-PEO-PCL linear triblock copolymers. The coincident or sequential crystallization of the PCL and PEO blocks was confirmed. Jiang et al.[29] observed the ring-banded spherulite morphology of the PEO-PCL diblock copolymer with the PEO weight fraction of 0.18.

In our previous study, the crystallization behavior and morphology of several PEO-PCL diblock copolymers (PEO-b-PCL) were studied. It was found that the crystallization behavior and morphology of PEO-b-PCL were obviously affected by the PCL/PEO weight ratio. A unique crystal morphology, the

* To whom correspondence should be addressed. Phone: +86-431-5262112. Fax: +86-431-5685653. E-mail: xschen@ciac.jl.cn.
† Chinese Academy of Sciences.
‡ Graduate School of Chinese Academy of Sciences.

10.1021/bm060578m CCC: $33.50
Published on Web 11/07/2006

concentric spherulite, was observed for PEO-b-PCL with WF_{PCL} of 0.50 (PEOCL50).[30,31] At the same time, the single-crystal morphology and structure of PEOCL50 was studied.[32] It was confirmed by electron diffraction (ED) that the coexistence of the two single-crystal layers formed from the two blocks. It is suggested from the previous results that the crystallization behavior and morphology of PEO-b-PCL will exhibit several interesting transitions by altering the PEO/PCL weight ratio. Further study of the detailed composition dependence should be valuable for disclosing the role of competition and confinement within the crystalline−crystalline block copolymer as well as for potential industrial application of the biodegradable copolymer. In this work, the crystallization behavior and morphology of PEO-b-PCL associated with the composition variation was studied in detail using differential scanning calorimetry (DSC), wide-angle X-ray diffraction (WAXD), temperature-dependent FTIR (TD-FTIR), and in situ polarized optical microscope (POM). In addition, the microdomain morphology and structure of PEO-b-PCL, which directly affected the degradation behavior of the copolymer, was characterized by small-angle X-ray scattering (SAXS).

2. Experimental Section

Materials. ϵ-Caprolactone (ϵ-CL, Aldrich) was purified by vacuo distillation over CaH_2. Monomethoxy poly(ethylene glycol) (mPEG5k, $M_n = 5000$ Da, $M_w/M_n = 1.04$, Alfa Aesar) was dried by an azeotropic distillation with dry toluene. Toluene was dried by refluxing over sodium metal under an argon atmosphere.

Polymerization. The PEO-PCL diblock copolymers (PEO-b-PCL) were synthesized by the ring-opening polymerization of ϵ-CL using mPEG5k as the macroinitiator and $Sn(Oct)_2$ as the catalyst. mPEG5k, ϵ-CL, and $Sn(Oct)_2$ (0.1 mol % of ϵ-CL) were weighed into an ampule flask equipped with a magnetic bar. Dry toluene was injected into the flask under an argon atmosphere. The flask was sealed under dry argon and immersed in an oil bath at 130 °C with stirring for 72 h. The product was purified by twice precipitating into cold isopropyl alcohol from chloroform solution and then dried in vacuo at room temperature for 24 h. The PCL homopolymer was synthesized using isopropyl alcohol as the initiator and $Sn(Oct)_2$ as the catalyst at 70 °C for 72 h.

Sample Preparation. The samples for POM observation were prepared by casting two drops of a 1 wt % chloroform solution of the polymer on a clean cover glass and then airing for 1 day, followed by drying in vacuo for 3 days.

Measurements. Proton nuclear magnetic resonance (^{1}H NMR) spectra of the polymers in deuterated chloroform solutions were recorded by a Bruker 300 MHz spectrometer with tetramethylsilane as internal standard. Gel permeation chromatography (GPC) was carried out using a Waters GPC instrument (515 HPLC pump) equipped with a Wyatt interferometer refractometer. Chloroform was used as the eluent at 25 °C, and the molecular weight was calibrated against poly(ethylene glycol) standards.

The crystallization temperatures T_c and melting points T_m of the PEO, PCL homopolymers and PEO-b-PCL were measured by a Perkin-Elmer 7 series thermal analysis system differential scanning calorimeter. Measurements during the first heating from −55 to 100 °C and then the first cooling from 100 to −55 °C as well as the second heating from −55 to 100 °C at 10 °C/min were performed. WAXD was carried out on a Rigaku X-ray diffractometer with a Ni-filtered Cu Kα radiation ($\lambda = 0.1546$ nm) at room temperature. The scan rate was 4 deg/min. The selected voltage and current were 40 kV and 200 mA, respectively. FTIR was carried out by a VERTEX 70 instrument. The pretreated sample was pressed into discs with KBr. TD-FTIR was performed by adding a temperature-controlled accessory. The sample was solution coated on the KBr plate and then cooled slowly from 70 °C at about 0.2 °C/min. Small-angle X-ray scattering (SAXS) measurement were performed on a Philips PW1700 equipped with a Kratky small-angle scattering camera, a step-scanning device, and a scintillation counter for recording the scattering intensity. Nickel-filtered Cu Kα radiation ($\lambda = 0.154$ nm) was supplied by an X-ray generator operated at 45 kV and 40 mA. The heat history of the sample for SAXS was as follows: first melted at 80 °C for 3 min, then cooled to 38 °C at 0.2 °C/min, and eventually remaining at 38 °C for 3 h. The scattering intensities were corrected for absorption, background scattering, and incident X-ray fluctuations of the samples. Crystal growth of the PEO, PCL homopolymers and PEO-b-PCL was observed under a polarized optical microscope (POM, Leica DMLP) equipped with a hot stage (Linkam) and a CCD video camera.

Table 1. Molecular Weight and Composition of PEO, PCL, and PEO-b-PCL

sample	M_n of PCL[a]	M_n of the polymer ($\times 10^3$)[b]	PDI[b]	content of PCL[a]
PEO5k	0	5	1.04	0
PEOCL16	920	6.65	1.04	0.16
PEOCL18	1100	7.24	1.24	0.18
PEOCL23	1510	7.48	1.24	0.23
PEOCL29	2000	8.07	1.08	0.29
PEOCL36	2800	8.54	1.07	0.36
PEOCL43	3840	8.92	1.07	0.43
PEOCL50	5090	9.81	1.16	0.50
PEOCL56	6240	10.8	1.09	0.56
PEOCL62	8130	13.7	1.36	0.62
PEOCL68	10 620	17.6	1.24	0.68
PEOCL77	17 000	24.1	1.29	0.77
PEOCL87	32 150	39.4	1.30	0.87
PEOCL93	64 600	55.8	1.63	0.93
PCL6k	5820	6.08	1.65	1
PCL30k	23 000	27.6	1.57	1

[a] Evaluated by ^{1}H NMR. [b] Determined by GPC (poly(ethylene glycol) standards), PDI = M_w/M_n.

3. Results and Discussion

Sample Characterization. The number-average molecular weight (M_n) of the PCL block in PEO-b-PCL was calculated by comparing the intensity of the characteristic peak of PCL (δ 2.28−2.33 ppm) with that of PEO (δ 3.65 ppm) in ^{1}H NMR spectra. The M_n of the PCL homopolymer was estimated by comparing the intensity of the characteristic peak of PCL (δ 2.28−2.33 ppm) with that of the isopropyl alcohol end group (δ 1.24−1.26 ppm). The M_n and polydispersity (PDI) of the sample were also characterized by GPC. As shown in Table 1, the molecular weight distributions of the obtained diblock copolymers were all narrow.

DSC, WAXD, and FTIR Characterization. The thermal behavior of several PEO-b-PCL diblock copolymers was characterized by DSC and WAXD in a previous study.[30] With increasing PCL/PEO weight ratio, T_c and T_m of PCL increased gradually while those of PEO greatly were reduced. However, it was hard to unambiguously distinguish T_c and T_m of each block only by DSC when the contents of PEO and PCL were close. As shown in Figure 1, there were double crystallization peaks in the DSC curves of PEO-b-PCL with WF_{PCL} of 0.29−0.87, except for PEOCL43, PEOCL50, and PEOCL56, which showed overlapping T_c and T_m of two blocks. WAXD and FTIR measurements (Figures 2−4) were performed to further analyze the crystallization behavior of PEO-b-PCL. It was suggested from the WAXD results that PEO and PCL had distinctly different cell unit and there was no eutectic or mixed crystals of the two components. T_c of the minor block of PEO-b-PCL

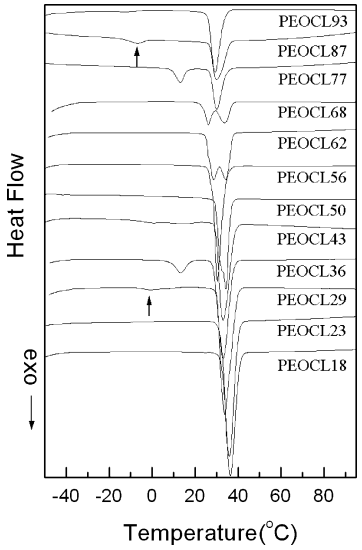

Figure 1. Cooling run of the DSC traces of PEO-b-PCL, 10 °C/min.

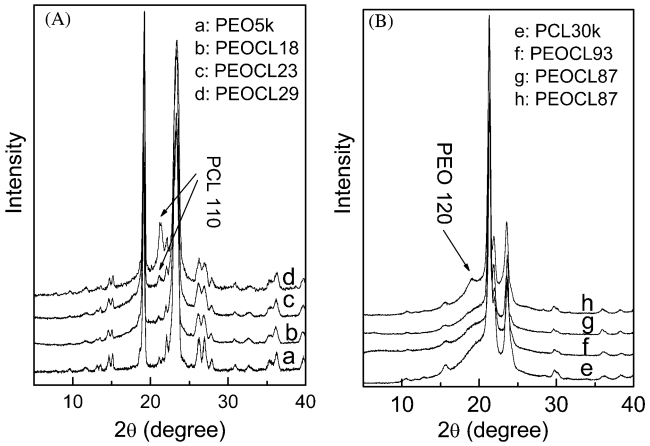

Figure 2. WAXD patterns (measured at room temperature) of PEO5k, PCL30k, and PEO-b-PCL. Sample preparation processes were as follows: samples a−f and h melt crystallized at 37 °C for 2 h and then crystallized at −20 °C for 48 h; sample g only melt crystallized at 37 °C for 20 min.

might be much lower than that of the homopolymer due to confinement.[30] The samples for WAXD and FTIR were pretreated in two steps: first crystallized at 37 °C for 2 h and then crystallized at −20 °C for 48 h. As shown in Figure 2A, for the sample with low PCL content an obvious PCL crystal diffraction peak for PEOCL29 and a quite weak one for PEOCL23 were observed. However, only a single crystallization (melting) peak for PEOCL16, PEOCL18, and PEOCL23 in the DSC traces, respectively, was observed, seemingly indicating that only PEO crystallized in them. Considering the insufficient sensitivity of DSC for detecting the very weak thermal behavior, FTIR was performed to analyze further the crystallization behavior of the samples. As shown in Figure 3, the characteristic vibrational bands corresponding to the PCL crystals at 710 and 731 cm^{-1} for PEOCL23 and PEOCL29 were observed,[31] but the typical peaks at 710 and 731 cm^{-1} for PEOCL18 were not observed. Therefore, it could be concluded that PCL in PEOCL23 and PEOCL29 was crystallizable, while PCL in PEOCL18 was uncrystallizable. In other words, the PCL block was uncrystallizable when WF_{PCL} was 0.18 or less in the diblock copolymers. Since the PCL homopolymer with M_n more than 500 was crystallizable,[38] the uncrystallizability of the PCL chain within PEOCL16 and PEOCL18 was due to confinement of the PEO block. For the sample with the low PEO content as

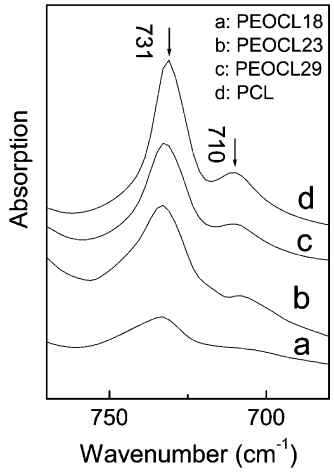

Figure 3. FTIR spectra of the PCL homopolymer and PEO-b-PCL. The samples first melt crystallized at 37 °C for 2 h and then crystallized at −20 °C for 48 h, followed by being pressed into discs with KBr.

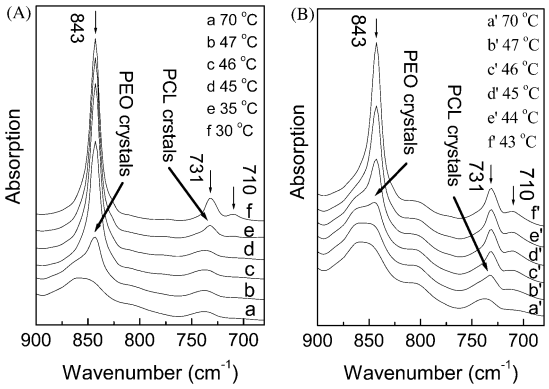

Figure 4. Temperature-dependent FTIR spectra of PEOCL36 (A) and PEOCL43 (B); the samples were solution coated on KBr plate.

shown in Figure 2B, the Bragg diffraction peak of the PEO crystallite was not observed in the WAXD spectrum of PEOCL93 crystallized at −20 °C. However, the obvious diffraction peak corresponding to the (120) plane of the PEO crystallite was observed in the WAXD spectrum of PEOCL87 crystallized at −20 °C for 48 h but not observed in the WAXD spectrum of PEOCL87 just crystallized at 37 °C for 20 min. Therefore, it could be concluded that the PEO block in PEOCL87 could only crystallize at low enough temperature, i.e., at large supercooling (−6.8 °C from DSC), while the PEO block in PEOCL93 was amorphous.

From analysis of WAXD, T_c and T_m of some samples could be directly assigned to the corresponding component. However, for the sample with the close block lengths, T_c and T_m of each block were very close and hard to be distinguished only by DSC and WAXD. Therefore, temperature-dependent FTIR (TD-FTIR) was carried out to further analyze the melt−crystallization behavior.

Temperature-Dependent FTIR (TD-FTIR). TD-FTIR was performed for PEOCL29, PEOCL36, PEOCL43, PEOCL50, PEOCL56, and PEOCL62. The vibrational bands at 843 and 731 cm^{-1} were chosen as the characteristic absorption of crystalline PEO and PCL, respectively.[31] The FTIR spectra of two typical samples are shown in Figure 4. During the cooling from melt at 0.2 °C/min for PEOCL36, the characteristic absorption of the crystalline PEO (843 cm^{-1}) began to emerge at 47 °C and almost stopped growing at 45 °C, while the characteristic absorption of the crystalline PCL (731 cm^{-1})

Table 2. Melting Point, Crystallization Temperature, and Heat of Fusion of the Samples

	T_c (°C)[a]		T_m (°C)[b]		ΔH_f (J/g)[b]	
sample	PEO	PCL	PEO	PCL	PEO	PCL
PEO5k	42.6		63.4, 56.9		168.5	
PEOCL16	35.3		58.9		121.1	
PEOCL18	36.4		62.6		121.6	
PEOCL23	35.9		61.4		120.5	
PEOCL29	33.9	−1.3	58.1	29.4	105.7	2.7
PEOCL36	33.0	13.4	57.1	38.5	88.3	5.6
PEOCL43	32.9		58.7		93.0	
PEOCL50	34.2		54.4		105.4	
PEOCL56	30.4		55.4		90.4	
PEOCL62	28.7	34.3		56.3	86.9	
PEOCL68	26.1	34.1	46.3, 50.4	55.5	35.5	46.2
PEOCL77	13.1	30.1	42.4	55.9	16.0	48.9
PEOCL87	−6.8	30.1	37.8	55.9	8.2	50.6
PEOCL93		29.4		58.9		45.1
PCL30k		34.1		60.5		60.2

[a] T_c: first cooling, 10 °C/min [b] T_m, ΔH_f: Second heating, 10 °C/min.

appeared at 35 °C. Therefore, it could be concluded that PEO in PEOCL36 crystallized first. However, during the cooling of PEOCL43, the characteristic absorption of the PCL crystals (731 cm^{-1}) emerged first at 47 °C, whereas the band of the PEO crystals (843 cm^{-1}) appeared later at 46 °C. This suggested that PCL crystals formed first in PEOCL43. Similarly, the melt−crystallization behaviors of PEOCL29, PEOCL50, PEOCL56, and PEOCL62 were analyzed by TD-FTIR. It could be concluded from the results that PEO crystals formed first from the melt in the sample with WF_{PCL} of 0.36 or less, while PCL crystals formed first in the sample with WF_{PCL} of 0.43 or more. Therefore, the confusing T_c and T_m in the DSC curves could be clearly assigned in terms of the TD-FTIR results. T_c, T_m, and the heat of fusion (ΔH_f) of each block are listed in Table 2. It was noticeable that during the cooling and heating run of DSC at 10 °C/min the crystallization and melting peaks were overlapping for samples with WF_{PCL} of 0.43−0.62 due to the quite near T_c and T_m of both blocks. As shown in Table 2, T_c and T_m of the PEO block decrease gradually, while those of the PCL block increase significantly with increasing WF_{PCL} of the copolymer.

The crystallinity X_c of PEO or PCL within PEO-b-PCL was evaluated from

$$X_c = \Delta H_f/(w\Delta H_f^\circ)$$

where w is the weight fraction of PEO or PCL and ΔH_f° is the heat of fusion for 100% crystalline PEO or PCL (assumed to be 135.3 and 213.7 J/g for PCL[39] and PEO,[40] respectively). The variations of the X_c of PEO and PCL plotted against WF_{PCL} are shown in Figure 5. The X_c of PEO within PEO-b-PCL was obviously lower than that of the PEO homopolymer even though the PCL block was very short. The X_c of PEO reduced continuously with the increase of the WF_{PCL}, and the declining rate of X_c of PEO seemed to be accelerated by the increase of WF_{PCL}. As shown in Figure 5, the reduction of X_c of PEO was relatively slow at the incipient stage, while it became sharp with the gradual increase of WF_{PCL}. On the other hand, the X_c of PCL increased rapidly with increasing WF_{PCL} from 0 to 0.68; however, it decreased gradually with the further increase of WF_{PCL}. It should be noted that there was a lack of X_c data of the samples with WF_{PCL} of 0.43−0.62. However, it is reasonable to believe that the variation of the X_c of PEO or PCL of the above samples should also accord with the traces shown in Figure 5.

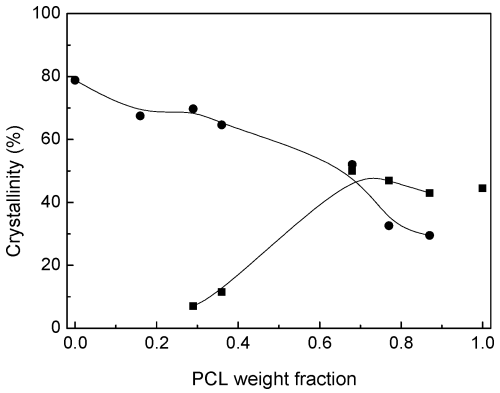

Figure 5. Crystallinity of PEO (●) and PCL (■) as a function of the PCL weight fraction.

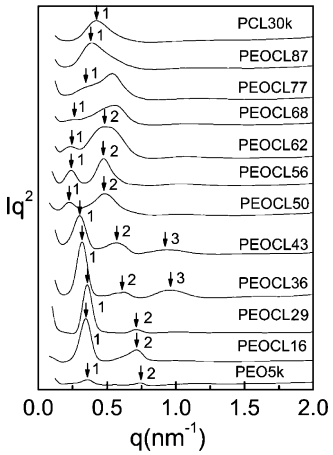

Figure 6. SAXS patterns of PEO5k, PCL30k, and PEO-b-PCL. All samples were measured at room temperature. The scattering vector $q = (4\pi/\lambda)\sin\theta$; 2θ is the scattering angle.

SAXS Measurement. The microdomain structures of PEO5k, PCL30k, and PEO-b-PCL were characterized by SAXS as shown in Figure 6. Multiple scattering peaks were observed for all samples except for PEOCL87 and PCL30k, suggesting a periodic microdomain structure with a long-range order.[41] The integer ratio of q at the scattering maxima indicated a lamellar structure. Since the morphological formation of the sample was driven by the crystallization and there were no eutectic or mixed crystals of the two components, the periodic system of PEO-b-PCL should consist of alternating PCL and PEO domains with both crystalline lamella and amorphous layers in each domain. The respective second-order reflection was more intense than the first one for PEOCL50, PEOCL56, PEOCL62, PEOCL68, and PEOCL77 because the scattering pattern contained contributions from the scattering of the lamellar structure of the whole periodic system and from the scattering of the semicrystalline PCL and PEO domains.[33,34] The relatively stronger second-order reflection also indicated that the principal scattering arose from the electronic density difference between the crystalline and amorphous layers of each species.[21,31] Additionally, the profiles of the second-order reflection for PEOCL62, PEOCL68, and PEOCL77 were distorted due to scattering from the semicrystalline PCL and PEO domains.[34] On the other hand, a strong and broad scattering peak was obtained in the SAXS curves for PEOCL87 and PCL30k, respectively.

The long period (L) of the sample was evaluated from the q value at the scattering maxima of the first-order reflection, and the total thickness of the crystalline PEO or PCL phase (d_c) was approximately evaluated according to the method of Floudas

Table 3. Crystallinity and Microdomain Structure Parameters of PEO, PCL, and PEO-b-PCL

		X_c^{DSC} (%)[b]		total thickness of respective crystalline phase d_c (nm)[c]	
sample	L (nm)[a]	$X_{c,PEO}$	$X_{c,PCL}$	PEO	PCL
PEO5k	17.0	78.8		13.4	
PEOCL16	18.2	67.5	0	11.5	
PEOCL29	17.8	69.7	7	10.7	
PEOCL36	19.3	64.6	11.5	10.3	
PEOCL43	20.7				
PEOCL50	28.6				
PEOCL56	26.3				
PEOCL62	25.7				
PEOCL68	24.6	51.9	50.2	7.0	5.6
PEOCL77	18.0	32.6	46.9	2.5	4.8
PEOCL87	16.2	29.5	43.0		5.0
PCL30k	14.7		44.5		6.6

[a] $L = q/2\pi$. [b] $X_c^{DSC} = \Delta H_f/(w\Delta H_f^\circ)$. [c] $d_{c,PEO} = L(N_{PEO}/(N_{PEO} + N_{PCL}))X_{c,PEO}$; $d_{c,PCL} = L(N_{PCL}/(N_{PEO} + N_{PCL}))X_{c,PCL}$.

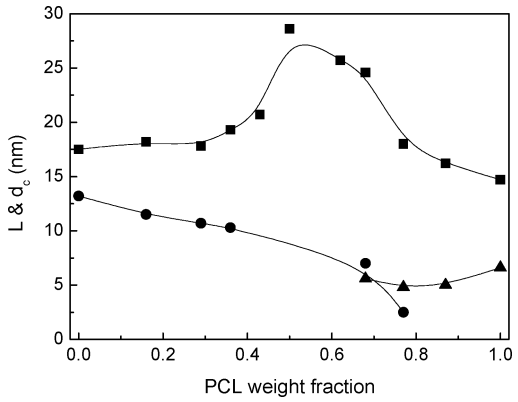

Figure 7. Long period (L, ■), total thickness of the crystalline PEO phase ($d_{c,PEO}$, ●), and PCL phase ($d_{c,PCL}$, ▲) within PEO, PCL, and PEO-b-PCL as a function of the PCL weight fraction.

et al. using the following equation[24]

$$d_c = X_c^{DSC} L N_{PEO(PCL)}/(N_{PEO} + N_{PCL})$$

where N_{PEO} or N_{PCL} is the degree of polymerization of the PEO or PCL block. L of PEO-b-PCL and d_c of each component are listed in Table 3. It was established that PEO with M_n near 5000 often crystallized into the once-folded or twice-folded form at a relatively large supercooling,[42,43] and the fold length of PEO5k was not affected obviously by the methyl end group.[44] The extended chain length of PEO can be calculated from $l = M_n/158.2$.[42] Therefore, the average extended chain length of PEO5k is 31.6 nm. From the L and $d_{c,PEO}$ of PEO5k and PEO-b-PCL with WF_{PCL} of 0.16−0.50 of this study it was suggested that the PEO block in the above cases should mainly crystallize into the once-fold form. The relationship between the microdomain structure (L and d_c) and WF_{PCL} is shown in Figure 7. The average thickness of the crystalline PEO phase $d_{c,PEO}$ was reduced gradually with increasing WF_{PCL} from 0 to 0.36. It was attributed to addition of the PCL block to the end of PEO, resulting in an irregular lamellar surface after crystallization.[21] However, the long period L of the whole copolymer increased slightly due to the amorphous layer thickness being thickened by the PCL chain. As WF_{PCL} increased from 0.36 to 0.50, L increased sharply, owing to the significant increase of the PCL domain thickness. However, L declined gradually with further increasing WF_{PCL} caused by the obvious depression of the PEO lamellar thickness. The reduction rate of L and $d_{c,PEO}$ was relatively slow with increasing WF_{PCL} from 0.50 to 0.68, while it became sharp when WF_{PCL} was greater than 0.68. On the other hand, the average thickness of the crystalline PCL phase $d_{c,PCL}$ was almost invariant with the increase of WF_{PCL} from 0.68 to 0.87.

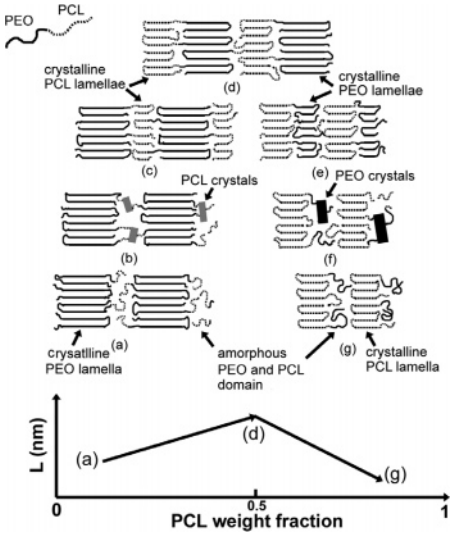

Figure 8. Schematic drawing of the variation of the microdomain structures of PEO-b-PCL with variation of the PCL weight fraction.

The schematic illustration of the microdomain structure of PEO-b-PCL is shown in Figure 8. When PEO was dominant in the diblock copolymer the crystalline lamellar thickness and crystallinity of PEO reduced slowly with increasing WF_{PCL}. When WF_{PCL} was low enough, the PCL chain was confined separately within the amorphous layers by the PEO crystalline lamellae and could not fold to crystallize (Figure 8a). With increasing its length, the PCL chain began to crystallize within the separately nanoscopic scale between the crystalline PEO lamellae at a large supercooling, which was related to fractionated crystallization (Figure 8b).[45] With further increasing the PCL chain length, the PCL crystalline lamellae with the relatively large size could form between the PEO crystalline lamellae, resulting in the significant increase of the crystallinity of PCL (Figure 8c). When WF_{PCL} was 0.43 or more, the PCL crystals were nucleated earlier and the thickness of the PCL lamellae increased obviously, resulting in confinement of the PEO block (Figure 8d). When PCL became the major component, the thickness of the PCL lamellae was almost invariant, even though the crystallinity of PCL declined gradually with increasing WF_{PCL} from 0.68 to 0.87, while the crystalline lamellar thickness and crystallinity of PEO were reduced significantly due to rapid depression of the crystallization capacity of the PEO block (Figure 8e). When WF_{PCL} is high enough (0.8 or more), the PEO chain was confined to crystallize within the separately nanoscopic scope at a large supercooling and eventually became amorphous (Figure 8f and g).

Spherulite Morphology and Growth. The isothermal crystallization at 36 °C of PEO5k, PCL6k and PEO-b-PCL was observed by hot-stage POM. It has been found that PCL could form the axialite morphology in ultrathin film (30−200 nm).[12,24] However, when crystallized in the thin film with a thickness of more than 200 nm at a relatively large supercooling, PCL would form the spherulite,[12] as was the case of this study. The POM morphology of each sample is shown in Figure 9. For samples with WF_{PCL} of 0.16−0.36, only the PEO spherulites were observed. On the other hand, only PCL spherulites were

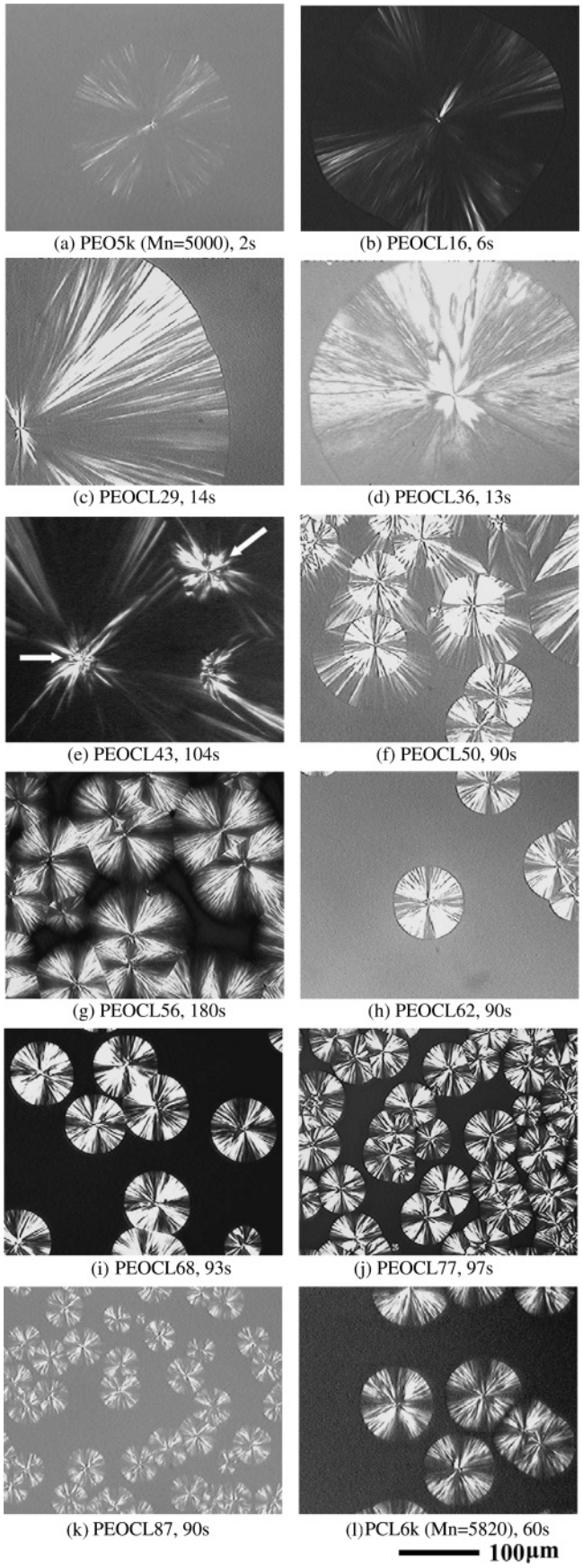

Figure 9. POM micrographs for the isothermal crystallization of PEO5k, PCL6k, and PEO-b-PCL; the samples were melted at 80 °C for 5 min and then quenched to 36 °C. The crystallization time for each graph is shown above the picture, and the moment when the temperature reached 36 °C was set as zero time.

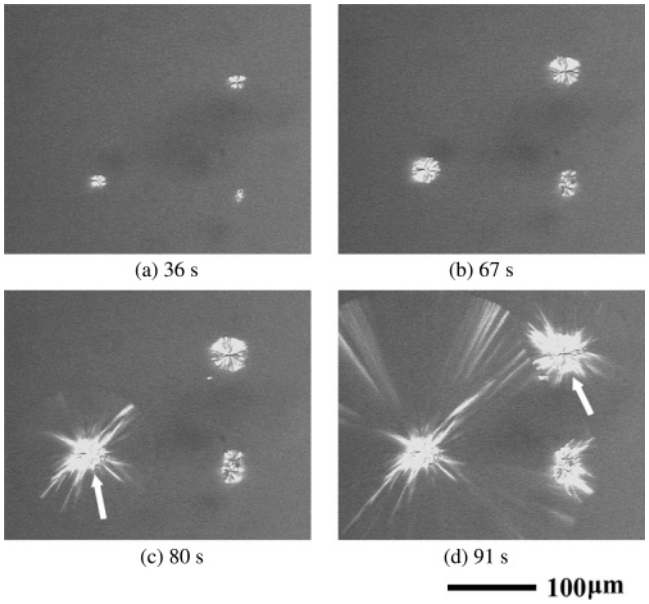

Figure 10. In situ POM micrographs of the isothermal crystallization of PEOCL43; the sample was melted at 80 °C for 5 min and then quenched to 36 °C.

observed for samples with WF_{PCL} of 0.56−0.87. In the previous study a unique concentric spherulite was observed for PEOCL50, and the formation mechanism was studied in detail.[30,31] In this study, we observed the crystal growth of PEOCL43 and PEOCL56 with WF_{PCL} close to that of PEOCL50. Similarly concentric spherulites were observed for PEOCL43, while only the PCL spherulites were observed for PEOCL56. It was identified by in situ microbeam FTIR that the morphology of the inner and outer portions of the concentric spherulites was determined by the PCL and PEO spherulites, respectively.[31] The real time growth of the concentric spherulites for PEOCL43 is shown in Figure 10. The PCL spherulites generated first and grew slowly. About 75 s later, PEO crystals were nucleated within some PCL spherulites one after the other (shown by the arrows in Figures 9e and 10c,d) and grew rapidly to form as the outer portion of the concentric spherulites. Because the crystal structures of PCL and PEO were different, the effect of the PCL crystals on PEO crystal nucleation might be small. PEO crystals should be nucleated on the same nuclei (e.g., dusts in the sample) for the PCL spherulites. Only in this case could the first formed double spherulite be concentric.

The radial variation of the PEO and PCL spherulites was plotted against the crystallization time as shown in Figure 11, and the spherulite growth rate G was obtained from the slope of the line. G of the PEO and PCL spherulites was affected obviously by the change of WF_{PCL} as shown in Figures 12 and 13. With increasing WF_{PCL} from 0 to 0.50, the growth rate of the PEO spherulites G_{PEO} declined sharply from 77.3 to 5.6 μm/s. However, the variation of the PCL spherulitic crystallization rate G_{PCL} exhibited a maximum rather than a monotonic change with increasing WF_{PCL} from 0.43 to 0.87. Because the PCL content in this study was raised by increasing M_n of the PCL chain, it might generate two main effects on the crystallization rate of PCL: one was to increase the PCL composition, which might raise G_{PCL},[46] while the other was to augment M_n of the PCL block, which would exhibit two opposite effects to G_{PCL} depending on the different M_n ranges. Chen et al. studied the spherulitic crystallization behavior of PCL with a wide M_n range of 1900−64700 in the temperature range of 35−43 °C.[47] It was pointed out by Chen and co-workers that the variation of the spherulite growth rate of the PCL homopolymers G_{PCLh}

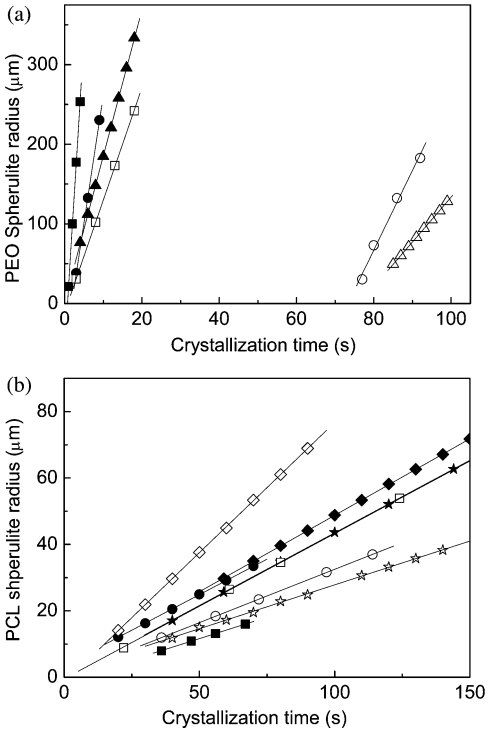

Figure 11. (a) Crystal growth of the PEO spherulite: ■, PEO5k; ●, PEOCL16; ▲, PEOPCL30, □; PEOCL36, ○; PEOCL43; △, PEOCL50. (b) Crystal growth of the PCL spherulite: ■, PEOCL43; ●, PEOCL50; ★, PEOCL56; ♦, PEOCL62; □, PEOCL68; ○, PEOCL77; ☆, PEOCL87; ◇ , PCL6k.

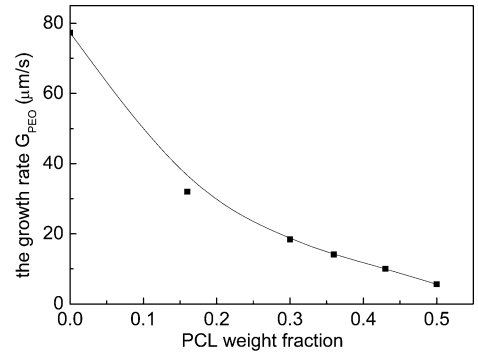

Figure 12. PEO spherulite growth rate G_{PEO} (■) as a function of the PCL weight fraction in PEO-b-PCL.

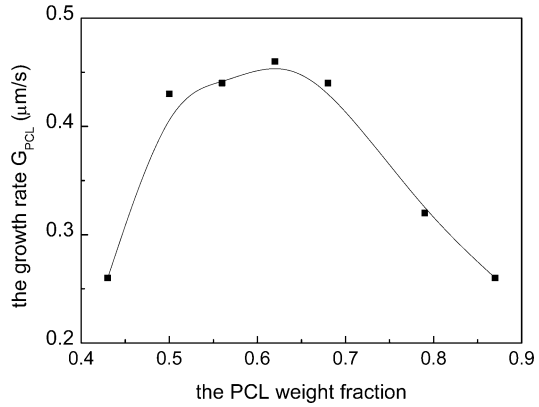

Figure 13. PCL spherulite growth rate G_{PCL} (■) as a function of the PCL weight fraction in PEO-b-PCL.

exhibited a maximum rather than a monotonic drop with the increase of M_n: G_{PCLh} rose with increasing M_n of PCL from 1900 to 6300 due to the increase of $T_m°$, while G_{PCLh} dropped gradually with further increasing M_n of PCL from 6300 to 64700 owing to the decrease of the segmental mobility.[47] The molecular weight dependence of the growth rate of crystallization was also studied by Hoffman for the polyethylene fractions.[48] It was established that the growth rate was approximately an inverse function of M_n as a result of reptation. In this work, G of PCL6k (M_n = 5820) and PCL8k (M_n = 8000) was measured to be 0.78 and 0.65 μm/s, respectively, which agreed well with the conclusion made by Chen and co-workers.[47] Therefore, with increasing WF_{PCL} from 0.43 to 0.56, i.e., $M_{n,PCL}$ from 3840 to 6240, G_{PCL} was promoted both by the PCL composition increase and by the increase of M_n of the PCL block. For samples with WF_{PCL} of 0.56−0.87, the further increase of M_n of the PCL block would retard G_{PCL}. However, G_{PCL} increased continuously until WF_{PCL} reached 0.62 ($M_{n,PCL}$ = 8130) as shown in Figure 13. This suggested that the effect of the PCL composition increase was still dominant in the sample with WF_{PCL} of 0.56−0.62.

In addition, the induction time of the PEO crystallites in the sample with WF_{PCL} of 0−0.36 was very short at 36 °C. However, it increased significantly in samples with WF_{PCL} of 0.43−0.50, and eventually no PEO spherulite was observed under POM in the sample with WF_{PCL} of 0.56 or more. On the other hand, the induction time of the PCL crystallites for samples with WF_{PCL} of 0.43−1 was very short at 36 °C.

From above analyses it was suggested that the covalently linked PEO and PCL blocks within PEO-b-PCL exhibited a significant influence on the crystallization behavior of each other. When one block crystallized first, crystallization of the other block was confined. The result was quite different from that of the PEO/PCL blends, which showed no obvious interaction between PEO and PCL.[21,49] Although the PEO/PCL blends were miscible in the amorphous phase,[50] the PEO/PCL blends formed the macrophase separation morphology due to the separated crystallization of two components.[27] However, crystallization of the PEO and PCL blocks within PEO-b-PCL was only allowed to take place within the covalently constrained microdomains, leading to the significantly mutual effects of both blocks and formation of the uniform macrophase morphology as the PEO spherulites, the PCL spherulites, or the concentric spherulites depending on the different composition.

Conclusions

The composition dependence of the crystallization behavior and morphology of PEO-b-PCL was significant. In this study M_n of the PEO block was fixed to be 5000, and WF_{PCL} was tailored by changing the PCL block length. Both blocks could crystallize in PEO-b-PCL with WF_{PCL} of 0.23−0.87; however, the crystallization temperature of each block highly depended on its content. During the cooling from melt at 0.2 °C/min, PEO crystallized first in the sample with WF_{PCL} of 0.36 or less. On the contrary, PCL crystallized first in the sample when WF_{PCL} was 0.43 or more. PEO crystallinity was reduced gradually with an increase of WF_{PCL}. PCL crystallinity increased significantly with increasing WF_{PCL} from 0.16 to 0.68; however, it declined gradually with further increasing WF_{PCL}. The long period of PEO-b-PCL increased gradually as WF_{PCL} increased from 0 to 0.50 due to the gradual increase of the PCL domain thickness; however, with further increasing WF_{PCL} from 0.50 to 0.87, the long period of the copolymer reduced significantly, owing to the obvious depression of the PEO crystalline lamellar thickness.

Crystal growth of PEO-b-PCL was observed by POM. When WF_{PCL} was 0.36 or less, only PEO spherulites were observed.

On the contrary, when the PCL WF_{PCL} was 0.56 or more, only PCL spherulites were observed. A unique concentric spherulite was observed for samples with WF_{PCL} of 0.43 and 0.50. The morphology of the inner and outer portions of the concentric spherulites was determined by the PCL and PEO spherulites, respectively. The growth rate of the PEO spherulites decreased sharply from 77.3 to 5.6 μm/s with increasing WF_{PCL} from 0 to 0.50. The growth rate of the PCL spherulites increased gradually from 0.26 to 0.46 μm/s with increasing WF_{PCL} from 0.43 to 0.62, but it was reduced from 0.46 to 0.26 μm/s with further increasing WF_{PCL} from 0.62 to 0.87.

Acknowledgment. This project was financially supported by the National Natural Science Foundation of China, National Fund for Distinguished Young Scholar (No. 50425309), and International Cooperation Fund of Science and Technology (Key project 2005DFA50290).

References and Notes

(1) Masahiko, O. *Prog. Polym. Sci.* **2002**, *27*, 87.
(2) Kathryn, E. U.; Scott, M. C.; Robert, S. L.; Kevin, M. S. *Chem. Rev.* **1999**, *99*, 3181.
(3) Albertsson, A. C.; Varma, K. *Biomacromolecules* **2003**, *4*, 1466.
(4) (a) Piao, L. H.; Dai, Z. L.; Deng, M. X.; Chen, X. S.; Jing, X. B. *Polymer* **2003**, *44*, 2025. (b) Tang, Z. H.; Chen, X. S.; Liang, Q. Z.; Bian, X. C.; Yang, L. X.; Piao, L. H.; Jing, X. B. *J Polym. Sci., Part A: Polym. Chem.* **2003**, *41*, 1934. (c) Tang, Z. H.; Chen, X. S.; Pang, X.; Yang, Y.; Zhang, X.; Jing, X. B. *Biomacromolecules* **2004**, *5*, 965.
(5) Li, S.; Garreau, H.; Pauvert, B.; McGrath, J.; Toniolo, A.; Vert, M. *Biomacromolecules* **2002**, *3*, 525.
(6) Na, Y. H.; He, Y.; Shuai, X. T.; Kikkwa, Y.; Doi, Y.; Inoue, Y. *Biomacromolecules* **2002**, *3*, 1179.
(7) Kikkwa, Y.; Iwata, T.; Inoue, Y.; Doi, Y.; *Biomacromolecules* **2002**, *3*, 350.
(8) Tsuji, H.; Tezuka, Y. *Biomacromolecules* **2004**, *5*, 1181.
(9) Tsuji, H.; Miyase, T.; Tezuka, Y.; Saha, S. K. *Biomacromolecules* **2005**, *6*, 244.
(10) Hamley, I. W.; Castelletto, V.; Castillo, R. V.; Muller, A. J.; Martin, C. M.; Pollet, E.; Dubois, P. *Macromolecules* **2005**, *38*, 463.
(11) Abe, H.; Harigaya, M.; Doi, Y. *Biomacromolecules* **2005**, *6*, 457.
(12) Mareau, V. H.; Prod'homme, R. E. *Macromolecules* **2005**, *38*, 398.
(13) Wang, J. L.; Dong, C. M. *Macromol. Chem. Phys.* **2006**, *207*, 554.
(14) Andronova, N.; Albertsson, A. C. *Biomacromolecules* **2006**, *7*, 1489.
(15) Yasin, M.; Tighe, B. J. *Biomaterials* **1992**, *13*, 9.
(16) Pitt, C. G. In *Biodegradable Polymers as Drug Delivery Systems*; Chasin, M., Langer, R., Eds.; M. Dekker: New York, 1990; p 71.
(17) Fujiwara, T.; Miyamoto, M.; Kimura, Y. *Macromolecules* **2000**, *33*, 2782.
(18) Ho, R. M.; Hsieh, P. Y.; Tseng, W. H.; Lin, C. C.; Lotz, B. *Macromolecules* **2003**, *36*, 9085.
(19) Sun, J. R.; Hong, Z. K.; Yang, L. X.; Tang, Z. H.; Chen, X. S.; Jing, X. B. *Polymer* **2004**, *45*, 5969.
(20) Muller, A. J.; Balsamo, V.; Arnal, M. L. *Adv. Polym. Sci.* **2005**, *190*, 1.
(21) Nojima, S.; Ono, M.; Ashida, T. *Polym. J.* **1992**, *24*, 1272.
(22) Gan, Z. H.; Jiang, B. Z.; Zhang, J. *J. Appl. Polym. Sci.* **1996**, *59*, 961.
(23) Gan, Z. H.; Zhang, J.; Jiang, B. Z. *J. Appl. Polym. Sci.* **1997**, *63*, 1793.
(24) Floudas, G.; Reiter, G.; Lambert, O.; Dumas, P. *Macromolecules* **1998**, *31*, 7279.
(25) Bogdanov, B.; Vidts, A.; Van Den Bulcke, A.; Verbeeck, R.; Schacht, E. *Polymer* **1997**, *39*,1631.
(26) Bogdanov, B.; Vidts, A.; Schacht, E. *Macromolecules* **1999**, *32*, 726.
(27) Shiomi, T.; Imai, K.; Takenaka, K.; Takeshita, H.; Hayashi, H.; Tezuka, Y. *Polymer* **2001**, *42*, 3233.
(28) Arnal, M. L.; Lopez-Carrasquero, F.; Laredo, E.; Muller, A. J. *Eur. Polym. J.* **2004**, *40*, 1461.
(29) Jiang, S. C.; He, C. L.; An, L. J.; Chen, X. S.; Jiang, B. Z. *Macromol. Chem. Phys.* **2004**, *205*, 2229.
(30) He, C. L.; Sun, J. R.; Deng, C.; Zhao, T.; Deng, M. X.; Chen, X. S.; Jing, X. B. *Biomacromolecules* **2004**, *5*, 2042.
(31) He, C. L.; Sun, J. R.; Zhao, T.; Hong, Z. K.; Zhuang, X. L.; Chen, X. S.; Jing, X. B. *Biomacromolecules* **2006**, *7*, 252.
(32) Sun, J. R.; Chen, X. S.; He, C. L.; Jing, X. B. *Macromolecules* **2006**, *39*, 3717.
(33) Ryan, A. J.; Hamley, I. W.; Bras, W.; Bates, F. S. *Macromolecules* **1995**, *28*, 3860.
(34) Hamley, I. W.; Fairclough, J. P. A.; Bates, F. S.; Ryan, A. J. *Polymer* **1998**, *39*, 1429.
(35) Hamley, I. W.; Fairclough, J. P. A.; Terrill, N. J.; Ryan, A. J.; Lipic, P. M.; Bates, F. S.; Towns-Andrews, E. *Macromolecules* **1996**, *29*, 8835.
(36) Quiram, D. J.; Register, R. A.; Marchand, G. R. *Macromolecules* **1997**, *30*, 4551.
(37) Zhu, L.; Cheng, S. Z. D.; Calhoun, B. H.; Ge, Q.; Quirk, R. P.; Thomas, E. L.; Hsiao, B. S.; Yeh, F.; Lotz, B. *J. Am. Chem. Soc.* **2000**, *122*, 5957.
(38) Ping, P.; Wang, W. S.; Chen, X. S.; Jing, X. B. *Biomacromolecules* **2005**, *6*, 587.
(39) Crescenzi, V.; Manzini, G.; Calzolari, G.; Borri, C. *Eur. Polym. J.* **1972**, *8*, 449.
(40) Queiroz, S. M.; Machado, J. C.; Porto, A. O.; Silva, G. G. *Polymer* **2001**, *42*, 3059.
(41) Chu, B.; Hsiao, B. S. *Chem. Rev.* **2001**, *101*, 1727.
(42) (a) Kovacs, A. J.; Gonthier, A. *Kolloid Z. Z. Polym.* **1972**, *250*, 530. (b) Kovacs, A. J.; Straupe, C.; Gonthier, A. *J. Polym. Sci.: Polym. Symp.* **1977**, *59*, 31.
(43) Cheng, S. Z. D.; Chen, J. H.; Barley, J. S.; Zhang, A.; Habenschuss, A.; Zschack, P. R. *Macromolecules* **1992**, *25*, 1453.
(44) Cheng, S. Z. D.; Wu, S. S.; Chen, J. H.; Zhou, Q.; Quirk, R. P.; Meerwall, E. D.; Hsiao, B. S.; Habenschuss, A.; Zschack, P. R. *Macromolecules* **1993**, *26*, 5105.
(45) Muller, A. J.; Balsamo, V.; Arnal, M. L.; Jakob, T.; Schmalz, H.; Abetz, V. *Macromolecules* **2002**, *35*, 3048.
(46) Guo, Q. P.; Groeninckx, G. *Polymer* **2001**, 8647.
(47) Chen, H. L.; Li, L. J.; Ou-Yang, W. C.; Hwang, J. C.; Wong, W. Y. *Macromolecules* **1997**, *30*, 1718.
(48) Hoffman, J. D. *Polymer* **1982**, 656.
(49) Lin, W. J.; Liu, C. H *J. Membr. Sci.* **2002**, *198*, 109.
(50) Kuo, S. W.; Lin, C. L.; Chang, F. C. *Macromolecules* **2002**, *35*, 278

BM060578M